Journal of Applied Polymer Science

Core–shell emulsion polymerization of styrene and butyl acrylate in the presence of polymerizable emulsifier

Ping Li, Zhiping Zhou, Weiwei Ma, Tongfan Hao
School of Materials Science and Engineering, Jiangsu University, Zhenjiang 212013, China
Correspondence to: Z. Zhou (E-mail: zhouzp@ujs.edu.cn)

ABSTRACT: A series of core–shell polymeric particles of styrene butyl acrylate were successfully prepared in the presence of polymerizable emulsifier. The compositions of the emulsions obtained were confirmed by Fourier transformed infrared spectrometry. Latexes and emulsion films were characterized by transmission electron microscopy and scanning electron microscopy, respectively. The thermostability of emulsion films was characterized by thermogravimetric analysis. The results showed that the existence of polymerizable emulsifier could enhance the solid content of the emulsion and the monomer conversion. The optimum mass ratio of polymerizable emulsifier to traditional emulsifier was 1:1, and the polymerizable emulsifier can participate in the emulsion polymerization perfectly. An emulsion with reverse core–shell particles exhibited better hydrophobic properties and thermostability than one with traditional core–shell particles. The film formed by the emulsion with reverse core–shell particles had lower water absorption, and it could be used in the fields of coatings, surface sizing agents, and spinning. © 2015 Wiley Periodicals, Inc. J. Appl. Polym. Sci. **2016**, *133*, 43091.

KEYWORDS: emulsion polymerization; films; polystyrene; surfactants

Received 15 June 2015; accepted 25 October 2015
DOI: 10.1002/app.43091

INTRODUCTION

Emulsifiers play an important role in fast nucleation in emulsion polymerization; they can scatter monomers into small droplets and form critical micelle that provide the site of polymerization. The traditional anionic emulsifiers and nonionic emulsifiers are widely used in industrial production. However, the traditional emulsifier molecules may migrate to the film surface and affect the waterproofness when an emulsion film is formed.[1,2] The polymerizable emulsifiers can copolymerize with the main monomers,[3–10] which can prevent the emulsifiers from desorbing from the emulsion particles. So, in recent years, an increasing number of researchers have begun to study polymerizable emulsifiers. Yan *et al.*[5] synthesized a polymerizable quaternary ammonium emulsifier and characterized its properties in a fiber crosslinking emulsion. It was effective in improving the stabilization of an emulsion with polymerizable emulsifier. Many researchers have also shown that the compounding of coemulsifiers with polymerizable emulsifiers promotes the stabilization of an emulsion because the coemulsifiers can rapidly reduce the surface tension of the oil–water interface. In addition, the charging sequence in the polymerization process is also an important factor that affects the emulsion performance. Usually, the particle size is somewhat large, and it has a wide size distribution in traditional emulsion polymerization.[11,12] Nevertheless, the core–shell emulsion polymerization can control particle size and its distribution perfectly. At the same time, it can also lower the film-forming temperature.[13] For the past few years, various types of emulsion particles have been synthesized by comparing the relative hydrophobicity of core-phase monomers and shell-phase monomers.[15–24] Traditionally, the hydrophobic monomers are taken as the core phase. Recently, a few of people have begun to explore emulsions with highly hydrophobic monomers as the shell phase. For example, Borthakur *et al.* prepared a series of core–shell polymeric particles with poly(*n*-butyl acrylate-*co*-methacrylic acid-*co*-ethylene glycol dimethylacrylate) as the core and poly(styrene-*co*-methyl methacrylate) as the shell. They observed that the core–shell morphology was distorted when the concentration of styrene in the shell composition was relatively high, which was attributed to the increase in the viscosity of the polymerization loci.[25] These core–shell latexes can potentially be applied as pigments in emulsion paint and would reduce the amount of TiO_2 used and hence afford a much more cost-effective method. Because the hydrophobic monomers have a better lipophilicity, they are more likely to spread into the core phase in which polymerization takes place. In this way, grafting and interfingering reactions can happen easily in the interface between the core phase and the shell phase, improving the compatibility of the core- and shell-phase polymers.[26–29]

In this article, we intend to prepare core–shell emulsions with butyl acrylate (BA) and styrene (ST) monomers in the presence

Table I. Material Components of Each Emulsion

Type	Core phase (g)	Shell phase (g)	DNS-86 (g)	Triton X-100 (g)	Initiator (g)	Buffer agent (g)	Crosslinking agent (g)	Water (g)	Particle size (nm)
E1	13 (St)	13 (BA)	0.6	1.8	0.3	1	0.3	60	235
E2	13 (St)	13 (BA)	0.8	1.6	0.3	1	0.3	60	192
E3	13 (St)	13 (BA)	1.2	1.2	0.3	1	0.3	60	154
E4	13 (St)	13 (BA)	1.6	0.8	0.3	1	0.3	60	145
E5	13 (St)	13 (BA)	1.8	0.6	0.3	1	0.3	60	139
E6	13 (BA)	13 (St)	0.6	1.8	0.3	1	0.3	60	211
E7	13 (BA)	13 (St)	0.8	1.6	0.3	1	0.3	60	172
E8	13 (BA)	13 (St)	1.2	1.2	0.3	1	0.3	60	135
E9	13 (BA)	13 (St)	1.6	0.8	0.3	1	0.3	60	132
E10	13 (BA)	13 (St)	1.8	0.6	0.3	1	0.3	60	130

of polymerizable emulsifier and coemulsifier by core–shell seeded emulsion polymerization. Poly(butyl acrylate) (PBA) was prepared first. Then, polystyrene (PS) was synthesized on the surface of the PBA particles. The PS obtained in the second stage spreads into the interior of the PBA particles and forms the core phase because it is more hydrophobic than the PBA. Compared with the traditional core–shell particles, in which the PS core is prepared first, the present particles are called reverse core–shell ones by some researchers.[30] The emulsion films prepared with the reverse core–shell particles are expected to be more waterproof and have better thermostability.

EXPERIMENTAL

Materials

Styrene, butyl acrylate, poly(ethylene glycol)-*tert*-octylphenyl ether (Triton X-100), and phosphotungstic acid (PTA) were purchased from Sinopharm Chemical Reagent Co., Ltd. (Beijing City, China). The polymerizable emulsifier, ammonium sulfate allyloxy nonyphenoxy poly(ethyleneoxy)(10) ether (DNS-86) was supplied by Guangzhou Shuangjian Trading Co., Ltd (Guangzhou, Guangdong Province, China) *N*-Methylol acrylamide (HMAM) was provided by Tianjin Chemical Reagent Research Institute (Tianjin City, China). Potassium peroxodisulfate (KPS) and sodium bicarbonate ($NaHCO_3$) were supplied by Zi Bo Yutao Chemical Co., Ltd. (Zibo City, Shandong Province, China). All of the chemicals were of analytical grade and used as supplied.

Synthesis of Latex

The experiment was conducted according to the pre-emulsifying monomers method. The pre-emulsion was prepared by adding DNS-86, Triton X-100, and ST (13.0 g) to a 100 mL three-neck round-bottom flask and stirring at 600 rpm for 1 h. The BA (13.0 g) was also pre-emulsified as above. The seed latex was prepared via semicontinuous emulsion polymerization. Deionized water (5.0 g), $NaHCO_3$ (1.0 g), HMAM (0.3 g), and 1/3 core phase pre-emulsion were added to a 500 mL three-neck round-bottom flask and stirred at 400 rpm under nitrogen atmosphere in a water bath. 1/3 of KPS solution (containing KPS 0.3 g and deionized water 15.0 g) was introduced to start the reaction when the system was heated to 75°C, and then the mixture was stirred for 30 min. The remaining pre-emulsified core-phase emulsion and 1/3 of KPS solution were dripped into the flask at a constant rate through two separate dropping funnels within 1.5 h, and then further stirring was conducted for 1 h at 80°C, and the seed latex was obtained. Afterwards, the shell-phase pre-emulsion and the remaining KPS solution were dripped into the flask within 2 h, respectively, and the mixture was stirred for another 2 h. Finally, the pH of the production was adjusted to 8–9 by ammonia ($NH_3{\cdot}H_2O$).

Formation of the Emulsion Film

A certain amount of the prepared emulsion was drawn into a 100 ml beaker, followed by a little of the polymerization inhibitor. Together they were measured as W_1. Then the beaker was put in the drying oven to remove the remaining monomers and other micromolecules. Thus the emulsion film was obtained. It was taken out when its weight stayed constant, which was measured as W_2. Afterwards, the deionized water was poured into the beaker to soak the film for 2 days. Ultimately, the film was dried by filter paper, which was measured as W_3.

The solid content (X) was calculated according to Equation (1), the monomer conversion (Y) was calculated by Equation (2),[31] and the water absorption (Z) was obtained from Equation (3)[32]:

$$X=\frac{W2-W0}{W1-W0}\times 100(\%) \tag{1}$$

where W_0 is the weight of the empty breaker and polymerization inhibitor.

$$Y=\frac{(W_2-W_0)/(W_1-W_0)-A}{B}\times 100(\%) \tag{2}$$

where A is the weight percent of the total nonvolatile ingredients in the recipe; B is the weight percent of the total monomer.

$$Z=\frac{W3-W2}{W2-W0}\times 100(\%) \tag{3}$$

By changing the charging sequence of monomers and the mass ratio of polymerizable emulsifier (DNS-86) to nonionic surfactant (Triton X-100), a series of core–shell latex particles were synthesized, the details of which are given in Table I.

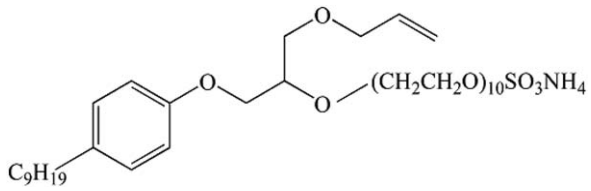

Figure 1. Structure of DNS-86.

Characterization Methods

Infrared spectrophotometry with a sample and potassium bromide was employed to record the infrared spectrogram ranging from 500 cm^{-1} to 4000 cm^{-1}. In order to eliminate small molecules, the sample was precipitated by ethyl alcohol before it was tested. A Nicolet Nexus 470 Fourier transformed infrared (FTIR) spectrometer (Madison, Wisconsin, US) was used to record the FTIR spectra.

The emulsion films dried on the glass slide before being sprayed on metal were employed to obtain scanning electron microscopy (SEM) images. An S-4800 field emission scanning electron microscope used to observe the morphology of emulsion films was purchased from Hitachi (Tokyo, Japan).

For the transmission electron microscopy (TEM) analysis, a JEM-2100 high-resolution transmission electron microscope supplied by JEOL (Tokyo, Japan) was used. The pH value of samples was adjusted to vary from 1.0 to 8.0, and the samples were embedded in an epoxy resin and cut into slices, stained by phosphotungstic acid.

Thermogravimetric analysis (TGA) and differential scanning calorimetry (DSC) data were obtained at a heating rate of 10°C min^{-1} from room temperature up to 550°C under argon atmosphere. The equipment was supplied by Perkin-Elmer (Waltham, Massachusetts, US).

A static water contact angle test was employed to evaluate the relative hydrophilicity or hydrophobicity of the samples. The sample was dropped onto the glass slide and dried in natural circumstances. Each sample was measured with a 2 μL drop of double-distilled water three times, and the average was taken. A KRÜSS DSA25 contact angle measuring device was supplied by KRÜSS(Hamburg, Germany).

RESULTS AND DISCUSSION

Analysis of the Polymerization Process

Table I presents the material components of each emulsion. It shows that the latex particle size decreases with the increasing content of polymerizable emulsifier (DNS-86). Because DNS-86 is a reactive anionic surfactant causing electrostatic repulsion and Triton X-100 is a nonionic one, the emulsion particles are negatively charged, and a structure with an electric double layer is formed. With the increasing content of DNS-86, the electronegativity and electrostatic repulsion of the emulsion particles is enhanced. However, DNS-86 has a lower critical micelle concentration (CMC) than traditional emulsifiers.[34] Thus, under the same conditions, the micelles emulsified by DNS-86 have a smaller size, which increases the specific surface area of the emulsion particles, and there were more emulsifiers bonded onto the surface of the emulsion particles. Therefore, the emulsion could retain a stable and dimensional homogeneity that was due to the presence of the DNS-86.

The content of polymerizable emulsifiers could affect not only the particle size but also the solid content and the monomer conversion. Figure 2 shows the relationships between the solid content of emulsions and the ratios of two kinds of emulsifiers in emulsions with traditional core–shell particles (a) and reverse ones (b). From the figure, it can be seen that the solid content of the emulsions first goes up and falls off subsequently with increasing content of DNS-86, and the solid content is the highest when the emulsifier ratio is 1:1. According to Equation (2), the monomer conversion is proportional to the solid content of the emulsions, so the variation trend of the conversion is correspondingly consistent with that of the solid content. It may be understood that DNS-86 is a weak electrolyte and contains ammonium sulfite ions, and the solution appears acidic. With the increasing content of DNS-86, the acidity of the solution is enhanced, which accelerates the decomposition of $K_2S_4O_8$. As a result, the solid content and monomer conversion are improved. But if its dose is excessive, the high H^+ concentration will lead to a high polymerization speed and high odds of collision or conglomeration among the latex particles. On the other hand, DNS-86 could be copolymerized with the monomers and embedded in the inner region of the particles, which weakens the stability. In addition, emulsions with reverse core–shell particles have a higher solid content and monomer conversion than that of normal core–shell particles with the same emulsifier ratio, which could be attributed to the fact that the reactivity ratio of BA/DNS-86 is lower than that of ST/DNS-86; in other words, the former has more opportunity to react with the polymerizable emulsifier (DNS-86) to form stable emulsion particles, so emulsions with reverse core–shell particles have a better polymerization efficiency and solid content.

Figure 3 shows the relationships between the water absorption of emulsion films and the emulsifier ratios in emulsions with traditional core–shell particles (a) and reverse ones (b). The results indicate that the water absorption is the lowest when the emulsifier ratio is 1:1 because the stability of the emulsion with

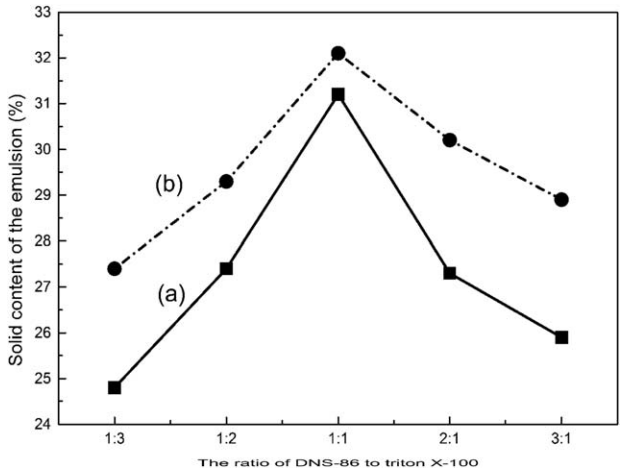

Figure 2. Relationships between the solid content of emulsion products and the emulsifier ratios for the (a) ST core phase and (b) BA one.

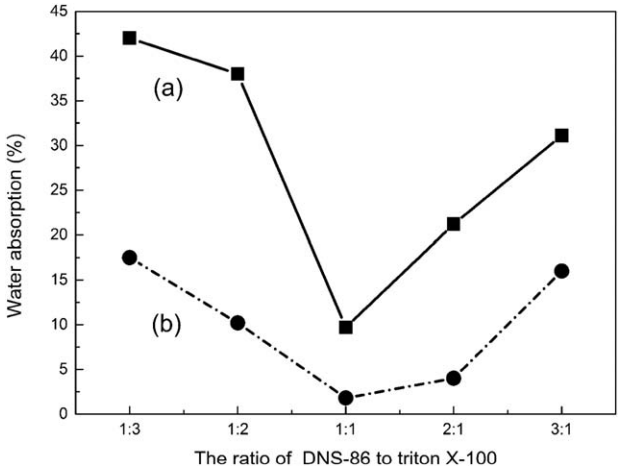

Figure 3. Relationships between the water absorption of emulsion films and the emulsifier ratios for the (a) ST core phase and (b) BA one.

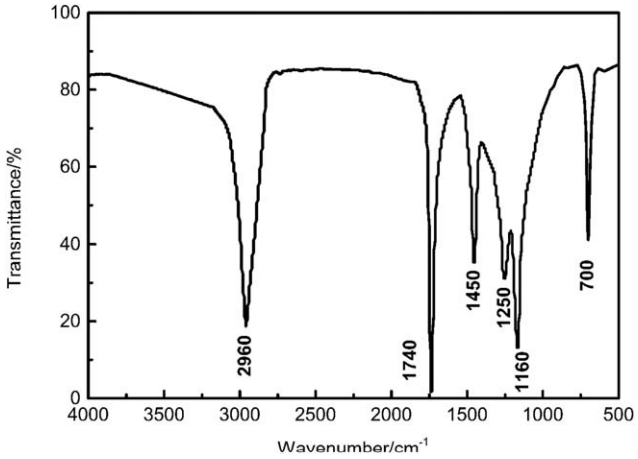

Figure 4. FTIR spectrum of emulsion E8.

a lower content of polymerizable emulsifier is very poor, which affects the performance of the emulsion film. However, the polymerizable emulsifier could be seen as a functional monomer that takes part in the polymerization if its content is very high. Because the emulsifiers have a high hydrophilic property, the waterproofness of the emulsion film could be lowered by excessive emulsifiers. Thus, the proper mixture ratio of DNS-86 to Triton X-100 is 1:1. Because of the influence of phase reversal, the reverse core–shell particles have higher hydrophobicity than do the traditional core–shell particles. Thus, highly hydrophobic products can be obtained through a core–shell seeded emulsion polymerization in which a polymer of hydrophobic monomers is synthesized in the second stage with an emulsifier ratio of 1:1.

FTIR Spectrum

The FTIR spectrum of the optimum sample (E8) is shown in Figure 4. The strong absorption band appearing at 2960 cm^{-1} corresponds to the methylene group (—CH_2—) within the butyl acrylate segment. The band at 1740 cm^{-1} is attributed to the stretching vibration of the ester group (C═O). The benzene ring frame vibration of styrene is located at 1450 cm^{-1} . The bands at 1250 cm^{-1} and 1160 cm^{-1} are due to the symmetric stretching vibrations of the carbon–oxygen–carbon bond (C—O—C). The absorption peak at 700 cm^{-1} is assigned to the stretching vibration of carbon–sulfur (C—S). Ultimately, the FTIR spectrum reveals that the monomers and the polymerizable emulsifier (DNS-86) have been introduced into the emulsion particles as desired through core–shell seeded emulsion polymerization.

Morphology of Latex Particles

Figure 5 shows the transmission electron microscopy (TEM) images of the E3 (A) and E8 (B) emulsion particles. In order to get different dyeing effects, the pH value of E3 was adjusted to 2.0 by diluted hydrochloric acid, and the pH value of E8 was regulated to 6.4 with a NaOH solution, correspondingly. Both of them were stained by PTA. In general, PTA mainly entered the PBA when the pH value was 2.0 (E3), but it existed in the form of sodium phosphotungstate when the pH was adjusted to 6.4 (E8). The solubility of sodium phosphotungstate in PS was much higher than in PBA.[27] Thus, the dark area in Figure 5(A)

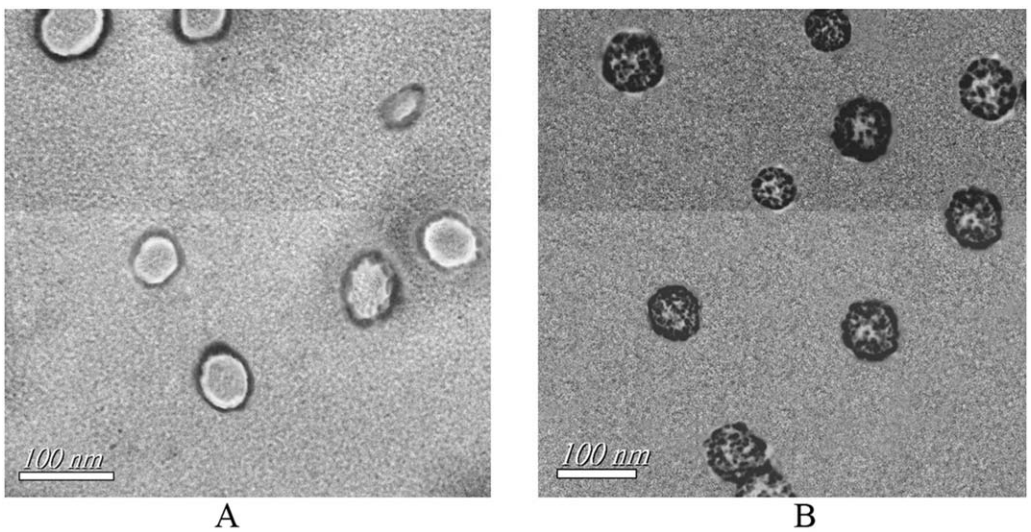

Figure 5. TEM micrograph of E3 and E8 latex samples embedded in epoxy resin; 109 × 55 mm (300 × 300 dpi).

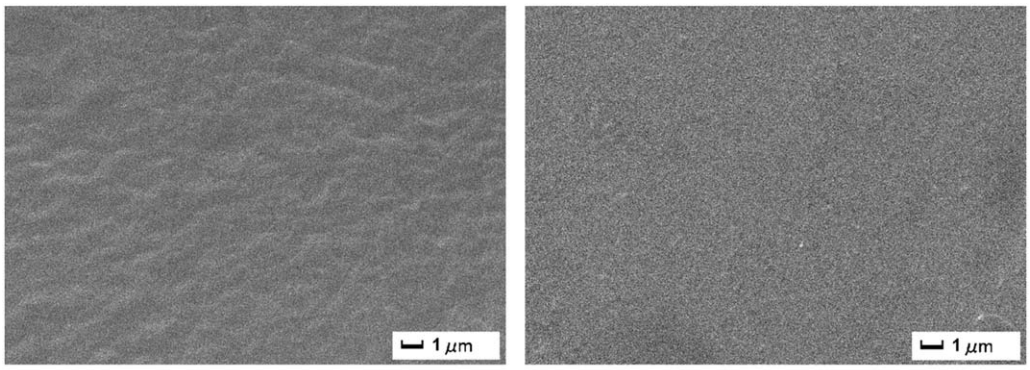

Figure 6. SEM micrograph of (A) E3 and (B) E8 emulsion films; 145 × 57 mm (300 × 300 dpi).

denotes PBA, while the dark area represents PS in Figure 5(B). The particles shown in Figure 5(A) have a traditional core–shell structure. However, the particles in Figure 5(B) look like sea islands and have a narrow particle size distribution. The peculiar structure (B) may be caused by the higher hydrophobic property of PS compared with PBA. In the polymerization process of E8, PS chains can spread into the interior and come to be the core of the latex particles, while PBA becomes the shell phase. In fact, only part of the PS extended to the interior of the latex particles because PBA also has a weak hydrophobic property. Thus, the island structure appeared. No matter which structure it is, the compatibility of the core or shell phase is improved by using self-crosslinking functional monomer *N*-methylol acrylamide (HMAM), which can copolymerize with other vinyl monomers to form an acrylate copolymer latex.[28] During the polymerization process, some active polymer chains of HMAM exist on the surface of the core particle. As result, graft copolymerization happened between the shell phase and the core phase. As shown in the literature, this type of sea-island structure is an equilibrium condition of particles with a reverse core–shell structure.[29,30] A similar type of structure has also previously been reported when using ST and MMA as monomers.[14]

Morphology of Emulsion Film and Latex Particles

Thin films were prepared by spin coating to investigate the film-forming property of the emulsions and the wetting behavior of the copolymers. The surface morphology of the emulsion films characterized by SEM is shown in Figure 6. It can be seen that the film formed by emulsion E8 (B) is very smooth without cracking, compared with the rough film formed by emulsion E3 (A). The wetting behavior was examined using deionized water by contact angle measurement, which has commonly been used as a criterion for the evaluation of hydrophobicity of a solid surface.[33] From Figure 7, we can see that the water contact angle of E3 (A) and E8 (B) emulsion films are 80.8° and 120.4°, respectively. The results show that the hydrophobicity of the emulsion film is significantly improved by the designed polymerization process (E8), in which the emulsion film prepared is abundant in the water-repellent benzene ring on the surface. Figure 8 presents the emulsion film formation process. During the film formation, the emulsion particles could be closely packed, due to their homogeneous size. With the volatilization of moisture, the capillary tube appears and the particle shape becomes distorted. Finally, polymer chains diffused mutually and a reticular polymer matrix formed in the presence of a crosslinking agent (HMAM). Because the particle size of E8 is smaller than that of E3, it is beneficial to form a close-packed structure. The emulsion film formed by E8 is smoother.

DSC and TG Analysis

As shown in Figure 9, two endothermic peaks could be easily seen in each DSC curve, which correspond to the decomposition of PBA and PS. However, the temperature intervals between the two peaks of E3 and E8 are different. The former is larger. Figure 10 shows their thermogravimetric curves. The initial decomposition temperature of E3 is 270°C, which is 25°C lower than that of E8. The half-life-period temperatures of the E3 and E8 samples are 419°C and 442°C, respectively. This phenomenon could be explained as follows. For the E3 sample, PS was surrounded by PBA. With the temperature increase, the side-chain radical departed primarily from PBA, and then the

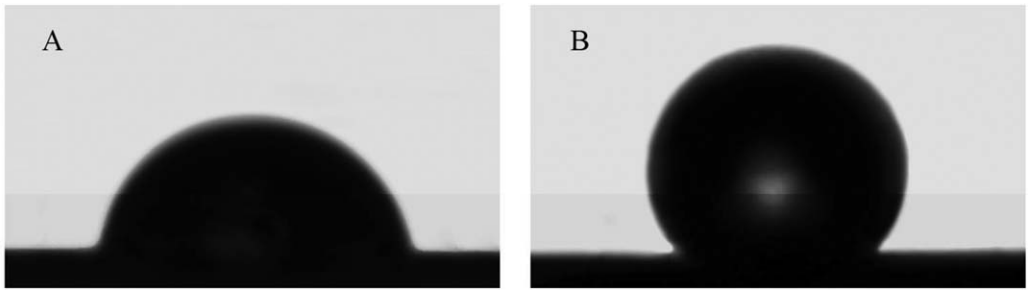

Figure 7. Water contact angle of (A) E3 and (B) E8 emulsion films; 150 × 39 mm (300 × 300 dpi).

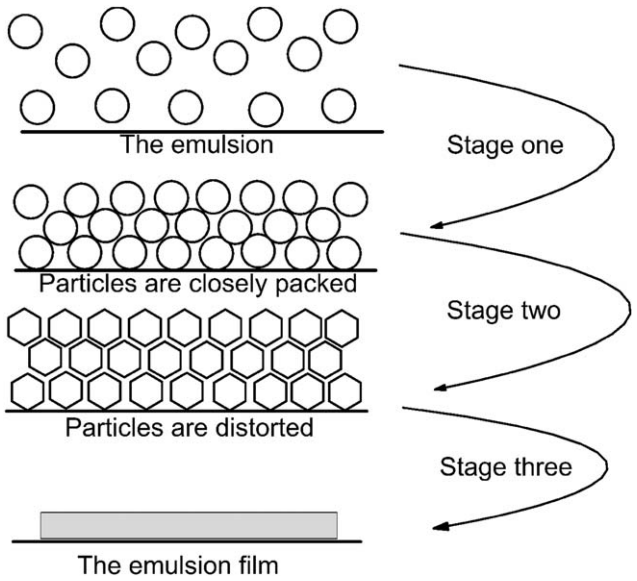

Figure 8. Schematic of emulsion film-forming process.

backbone of PBA was broken. Compared with E3, the PS in the sample E8 was depolymerized first. Because the decomposition temperature of PS is higher than that of PBA, the emergence of the first endothermic peak of E8 is later than that of E3. Along with the decrease in polymerization degree of PS, the chains of PBA begin to diffuse and break down under a higher-temperature atmosphere. The existence of the decomposed PBA fragments was beneficial to the stabilization of the benzene ring. Thus, the thermal stability of the E8 sample is higher than that of the E3 sample because of the difference in the charging procedure.

CONCLUSIONS

Two kinds of core–shell particles were prepared with styrene and butyl acrylate monomers, and their properties were compared. For one, the PS was prepared first and then the shell-phase PBA was synthesized; these are the traditional core–shell particles. For the other, PBA particles were obtained first and then PS was grafted onto it, thus forming the reverse core–shell particles. The use of a polymerizable emulsifier improved the solid content of the emulsion and the monomer conversion. The optimum mass ratio of the two kinds of emulsifiers was 1:1. FTIR spectra analysis confirmed that the polymerizable emulsifier (DNS-86) could be bonded to the emulsion particles. The reverse core–shell structure was seen by TEM images. SEM showed that the emulsion with novel reverse core–shell particles had a better film-forming property, by which the film formed has lower water absorption. Furthermore, DSC and TG analyses revealed that the emulsion with reverse core–shell particles exhibited more excellent thermostability. This novel emulsion film prepared with the reverse core–shell particles could be used in the fields of coatings, surface sizing agents, and spinning.

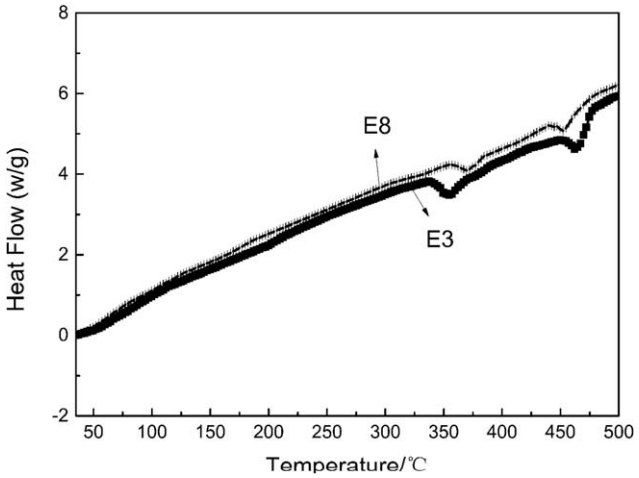

Figure 9. Thermograms of samples E3 and E8.

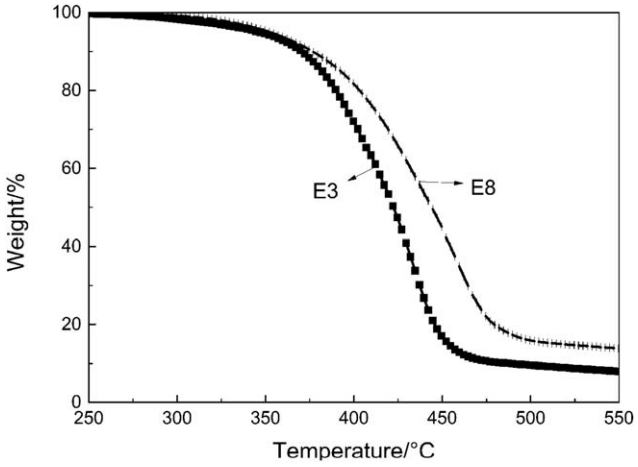

Figure 10. TGA curves of samples E3 and E8.

ACKNOWLEDGMENTS

This work was sponsored by the National Natural Science Foundation of China (21174057) and the National Basic Research Program of China (973 Program, 2012CB821500).

REFERENCES

1. Guyot, A. *Macromol. Symp.* **2002**, *179*, 105.
2. López-Aguilar, J. E.; Vargas, R. O.; Escobar-Toledo, C. E.; Mendizábal, E.; Puig, J. E.; López-Serrano, F. *J. Appl. Polym. Sci.* **2015**, *132*, 41720.
3. Reb, P.; Margarit, K.; Puri, M. J. *Macromolecules* **2000**, *33*, 7718.
4. Xu, X. J.; Goh, H. L.; Siow, K. S. J. *Langmuir* **2001**, *17*, 6077.
5. Yan, X. H.; Ji, Y. X.; Xu, W.; Sao, R. *Colloids Surf. A: Physicochem. Eng. Asp.* **2014**, *443*, 60.
6. Guyot, A.; Tauer, K.; Asua, J. M.; VanEs, S. *Acta Polym.* **1999**, *50*, 57–66.
7. Samakande, A.; Hartmann, P. C.; Sanderson, R. D. J. *Colloid Interface Sci.* **2006**, *296*, 316.

8. Zana, R. *Adv. Colloid Interface Sci.* **2002**, *97*, 205.
9. Bunio, P.; Chlebicki, J. *Colloids Surf. A: Physicochem. Eng. Asp.* **2012**, *413*, 119.
10. Martinez, A.; Gonzalez, C.; Porras, M.; Gutierrez, J. M. *Colloids Surf. A: Physicochem. Eng. Asp.* **2005**, *270*, 67.
11. Zhang, R. L.; Liu, Y.; Huang, Y. D.; Liu, L. *Appl. Surf. Sci.* **2013**, *287*, 423.
12. Samyn, P.; Deconinck, M.; Schoukens, G.; Stanssens, D. *Prog. Org. Coat.* **2010**, *69*, 442.
13. Yuan, J. J.; Qian, H. J. *Appl. Polym. Sci.* **2015**, *132*, 42003.
14. Jonsson, J. E.; Karlsson, O. J.; Hassander, H.; Tornell, B. *Eur. Polym. J.* **2007**, *43*, 1322.
15. Peng, C. A.; Da, J.; Hsu, Y. C.; Hogen-Esch, T. E. J. *Disper. Sci. Technol.* **2006**, *27*, 377.
16. Karlsson, O. J.; Stubbs, J. M.; Carrier, R. H.; Sundberg, D. C. *Polym. React. Eng.* **2003**, *11*, 589.
17. Niranjan, P. S.; Upadhyay, S. K. J. *Disper. Sci. Technol.* **2011**, *32*, 109.
18. Ma, J. Z.; Liu, Y. H.; Bao, Y.; Liu, J. L. *Adv. Colloid Interface* **2013**, *197–198*, 118.
19. Yang, S. F.; Xiong, P. T.; Gong, T.; Lu, D. P. *Eur. Polym. J.* **2005**, *41*, 2973.
20. Zhang, Y. F.; Zhang, R.; Yang, C. L.; Xu, J. *Colloids Surf. A: Physicochem. Eng. Asp.* **2013**, *436*, 549.
21. Alyamac, E.; Soucek, M. D. *Prog. Org. Coat.* **2011**, *71*, 213.
22. Chen, Y. J.; Zhang, C. C.; Chen, X. X. *Eur. Polym. J.* **2006**, *42*, 694.
23. Yao, W. Q.; Li, Y. J.; Huang, X. Y. *Polymer* **2014**, *55*, 6197.
24. Chen, L. J.; Shi, H. X.; Wu, H. K.; Xiang, J. P. *Colloids Surf. A: Physicochem. Eng. Asp.* **2010**, *368*, 148.
25. Borthakur, L. J.; Jana, T.; Dolui, S. K. J. *Coat. Technol. Res.* **2010**, *7*, 765.
26. Min, T. I.; Klein, A.; EI-Aasser, M. S. *Org. Coat. Appl.* **1981**, *46*, 314.
27. Li, X. Q.; Chen, P. Z.; Qin, C. H. *Polym. Mater. Sci. Eng.* **1999**, *15*, 129.
28. Xu, W.; An, Q. F.; Hao, L. F.; Zhang, D.; Zhang, M. *Appl. Surf. Sci.* **2013**. *268*, 373.
29. Karlsson, L. E.; Karlsson, O. J.; Sundberg, D. C. *J. Appl. Polym. Sci.* **2003**, *90*, 905.
30. Chai, S. L.; Jin, M. M.; Tan, H. M. *Eur. Polym. J.* **2008**, *44*, 3306.
31. Yin, N. W.; Chen, K. Q. *Polymer* **2004**, *45*, 3587.
32. Abele, S.; Zicmanis, A.; Graillat, C.; Guyot, A. *Langmuir* **1999**, *15*, 1045.
33. Deng, X.; Liu, B.; Cao, S.; Luo, R.; Chen, H. *Appl. Surf. Sci.* **2007**, *253*, 4823.
34. Li, H. Q.; Ren, X. K.; Lai, X. J.; Zeng, X. R. J. *Coat. Technol. Res.* **2014**, *11*, 959.